

# High-frequency response of a two-dimensional electron system under microwave irradiation

I. V. Andreev\* and V. M. Muravev

*Institute of Solid State Physics RAS, Chernogolovka, RU-142432, Russia*

I. V. Kukushkin

*Institute of Solid State Physics RAS, Chernogolovka, RU-142432, Russia and*

*Max-Planck-Institut für Festkörperforschung, Heisenbergstraße 1, DE-70569 Stuttgart, Germany*

S. Schmutz and W. Dietsche

*Max-Planck-Institut für Festkörperforschung, Heisenbergstraße 1, DE-70569 Stuttgart, Germany*

(Received 26 January 2011; revised manuscript received 16 February 2011; published 21 March 2011)

In this paper, the high-frequency ( $f = 0.05\text{--}10\text{ GHz}$ ) magnetoresistance of a two-dimensional electron system is studied in the regime of microwave-induced resistance oscillations (MIRO). For this purpose, we employed a technique based on measuring the attenuation of a broadband coplanar transmission line placed on the sample surface, with the sample simultaneously being subjected to external microwave irradiation of frequency  $F = 40\text{--}140\text{ GHz}$ . In the  $f \leq 1\text{ GHz}$  probe frequency range, the coplanar waveguide transmission exhibits several features that repeat the MIRO measured on the same sample using the conventional dc transport technique. At higher probe signal frequencies  $f$ , the MIRO features in transmission are significantly suppressed. In particular, for a microwave irradiation frequency of  $F = 80\text{ GHz}$ , the first two features of the waveguide transmission decrease by an order of magnitude at  $f_1 = 3.0\text{ GHz}$  and  $f_2 = 1.5\text{ GHz}$ , respectively.

DOI: 10.1103/PhysRevB.83.121308

PACS number(s): 73.23.-b, 73.63.Hs, 72.20.My, 73.50.Mx

Since their discovery, microwave-induced magnetoresistance oscillations (MIRO) in two-dimensional electron systems (2DES) have been the subject of comprehensive research.<sup>1,2</sup> The attention drawn is largely attributed to a wide variety of remarkable peculiarities, including the phenomenon of zero resistance states at the oscillation minima,<sup>3,4</sup> the nonsensitivity to microwave polarization,<sup>5</sup> the observation of alternating photovoltage oscillations,<sup>6</sup> and the disappearance of oscillations in comparatively small magnetic fields parallel to the sample surface.<sup>7</sup> The nature of these phenomena remains a mystery and a subject of discussion.<sup>8-12</sup>

Thus far, all experimental observations of MIRO have been limited to direct current (dc) measurements.<sup>1,3-6,13-15</sup> However, recent high-frequency contactless studies of MIRO using coplanar,<sup>16</sup> resonator,<sup>17</sup> and capacitive<sup>6,18,19</sup> techniques have produced controversial results. The controversies are speculated to originate from the fact that all the experiments were limited to very narrow frequency ranges of the probe signal. As a consequence, a comprehensive physical picture of the MIRO kinetics and the contribution of electron density nonuniformity regions to the origin of the oscillations could not be provided.

We have managed to overcome these limitations using a broadband coplanar waveguide technique.<sup>20</sup> In our experiments, we measure the attenuation of a high-frequency probe signal propagating along the coplanar waveguide that has been lithographically patterned onto the sample surface. This technique enables the study of the 2DES magnetotransport properties over a frequency range up to several tens of gigahertz.<sup>20</sup> Specifically, this technique allowed us to study the high-frequency response of 2DES to MIRO at probe signal frequencies ranging between 0.05 and 10 GHz. It was also possible to demonstrate that the frequency of the probe signal has a pronounced effect on the MIRO amplitude.

The experiments are performed on GaAs/AlGaAs quantum wells fabricated by molecular beam epitaxy. Structures with electron densities of  $n = (1.3\text{--}2.8) \times 10^{11}\text{ cm}^{-2}$  and mobilities  $\mu = (6\text{--}15) \times 10^6\text{ cm}^2/(\text{V s})$  at temperature of  $T = 1.5\text{ K}$  were studied. The samples including a Hall bar with a coplanar waveguide deposited on the top of the mesa are defined by means of optical lithography. The coplanar waveguide<sup>21</sup> is a type of a strip line that consists of a narrow central metal strip deposited onto a substrate (a GaAs/AlGaAs heterostructure in our case) between two grounded wide planes (inset of Fig. 1). The length of the coplanar waveguide is  $d = 800\text{ }\mu\text{m}$ , while the width of its central strip is  $a = 44\text{ }\mu\text{m}$  and the distance between grounded planes is  $b = 104\text{ }\mu\text{m}$ . The parameters of the waveguide are chosen such that its characteristic impedance is  $Z_0 = 50\text{ }\Omega$ . As a high-frequency probe signal passes through the coplanar waveguide, the observed power losses mainly originate from heating the 2DES by the electric field concentrated in the slots of the coplanar waveguide. The relative coplanar waveguide transmission  $\mathcal{T}$  is determined by its geometric parameters and the diagonal component of the 2DES conductivity tensor  $\sigma_{xx}$  (Ref. 20):

$$\mathcal{T} = \exp\left(-\frac{Z_0 \operatorname{Re}(\sigma_{xx})d}{w}\right), \quad (1)$$

where  $w = (b - a)/2$  is the slot width between the central strip and the side grounded planes and  $\operatorname{Re}(\sigma_{xx})$  denotes the real part of conductivity  $\sigma_{xx}$ . This expression is valid at small lateral dimensions  $a$  and  $b$ , as well as at small distances between the 2DES and the waveguide deposited on the heterostructure as compared to the microwave signal wavelength. Therefore, the 2DES magnetotransport characteristics can be determined by measuring the coplanar waveguide transmission. In the case of this contactless technique, the coplanar waveguide is connected by means of  $50\text{-}\Omega$  coaxial cables in series with

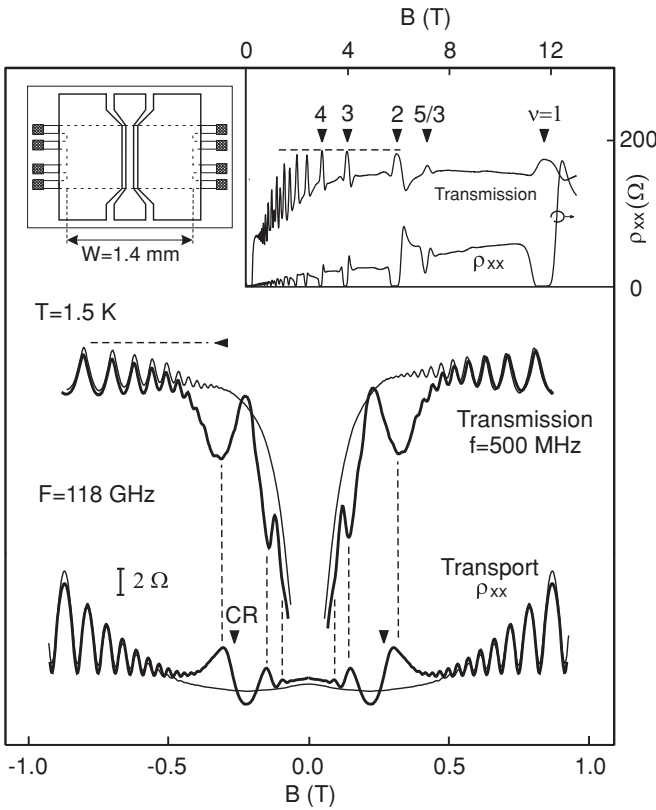


FIG. 1. Comparison of the 2DES magnetotransport characteristics in the absence (thin curves) and presence (thick curves) of microwave irradiation with a frequency of  $F = 118$  GHz. The upper curves correspond to coplanar waveguide transmission and the lower curves to dc magnetoresistance. The vertical arrows indicate the position of the magnetic field corresponding to the cyclotron resonance (CR). The inset shows a comparison of results obtained by means of contactless high-frequency and conventional contact techniques for a wide magnetic field range in case of no external microwave irradiation. The lower curve represents the dc magnetoresistance of 2DES, and the upper curve represents the coplanar waveguide transmission signal at a probe signal frequency of  $f = 400$  MHz. A schematic drawing of the sample (top view) is also shown. Crosshatching indicates ohmic contacts, and bold lines are boundaries of the coplanar waveguide metallization.

the high-frequency probe signal generator ( $f = 0$ – $20$  GHz) and the detector, where the latter is a Schottky diode placed outside the cryostat. The power of the generator does not exceed 100 nW. It is modulated at a frequency of 810 Hz, and the output signal is detected using a standard lock-in technique. When using the transport technique, a 0.1- $\mu$ A and 13-Hz ac current passes through the Hall bar shaped beneath the coplanar waveguide. Magnetoresistance is measured at the same frequency using the same lock-in technique. The sample is fixed at the end of a rectangular waveguide with a cross section of  $7 \times 3.5$  mm $^2$  and immersed into the cryostat with a superconducting magnet. The magnetic field is directed normal to the sample surface. The helium vapor is pumped out to attain a temperature of  $T = 1.5$  K. To study 2DES in the MIRO regime, the sample is exposed via the rectangular waveguide to microwave radiation in the frequency range from 40 to 140 GHz with input power not exceeding 1 mW.

The inset in Fig. 1 shows the performance of the high-frequency coplanar technique. The upper curve corresponds to the coplanar waveguide transmission at probe signal frequency of  $f = 400$  MHz, while the lower curve represents the magnetoresistance measured at dc using the transport technique. All the transport measurements were performed on the Hall bar of width  $W = 1.4$  mm located beneath the coplanar waveguide used for contactless measurements (see schematic in Fig. 1). It is clearly seen that, over a wide magnetic field range, the contactless high-frequency technique ensures true reproduction of all the characteristic features seen in magnetotransport of the 2DES. Figure 1 shows the magnetic field dependences of the Hall bar resistivity  $\rho_{xx}$  and the coplanar waveguide transmission measured as the sample was exposed to microwave irradiation with a frequency of  $F = 118$  GHz. Thin curves represent the magnetic field dependence in the absence of microwave irradiation. It is clearly seen that, in the case of exposure to microwave irradiation and relatively small magnetic fields, both the dc magnetoresistance and the coplanar waveguide transmission exhibit a number of additional features. As it will be shown below, the peculiarities observed correspond to the so-called microwave-induced  $1/B$  periodic resistance oscillations (MIRO).<sup>1,2</sup> The magnetic field values of all different features in the case of the coplanar waveguide transmission coincide exactly with those of the dc magnetotransport. These are marked by dashed lines. On the other hand, vertical arrows denote the position of the cyclotron resonance, which corresponds to a slightly lower magnetic field than the first MIRO maximum is observed in the 2DES magnetoresistivity.

To confirm the assumption that the peculiarities observed are related to multiple harmonics of the cyclotron resonance,<sup>1</sup> the experiments shown in Fig. 1 were repeated for a greater number of microwave irradiation frequencies. The results obtained are shown in Fig. 2. As it can be clearly seen in Fig. 2(a), the position of the magnetic field-dependent features in the case of coplanar waveguide transmission at 500 MHz varies with the microwave irradiation frequency, whereas features related to Shubnikov-de Haas oscillations remain unchanged. Figure 2(b) shows the magnetodispersion of the transmission signal minima (circles), as well as the corresponding magnetoresistance maxima (diamonds) measured using the transport technique. It is clearly seen that the microwave irradiation frequency at which magnetic field-dependent features are observed do linearly depend on the magnetic field magnitude. The experimental points follow multiple harmonics of cyclotron resonance  $2\pi F = \omega = i\omega_c = ieB/m^*$  (dashed lines), where the  $i$  factor denotes the harmonic number,  $e$  and  $m^*$  are electron charge and effective mass, respectively, and  $B$  is the magnetic field magnitude. Note that the first MIRO maxima position is shifted from cyclotron resonance in agreement with previous MIRO research,<sup>4,22</sup> but, for the higher maxima, such shift is not observed. This fact may imply that the data could not be described using the effective electron mass  $m^* = 0.067m_0$  (see also Ref. 22). Furthermore, the magnitude of the magnetic field at which transmission minima are observed coincides with that of the magnetoresistance maxima. Therefore, we conclude that the experimentally observed features of coplanar waveguide transmission at a probe signal frequency of  $f = 500$  MHz correspond to MIRO.<sup>1,2</sup> Thus, the results presented above

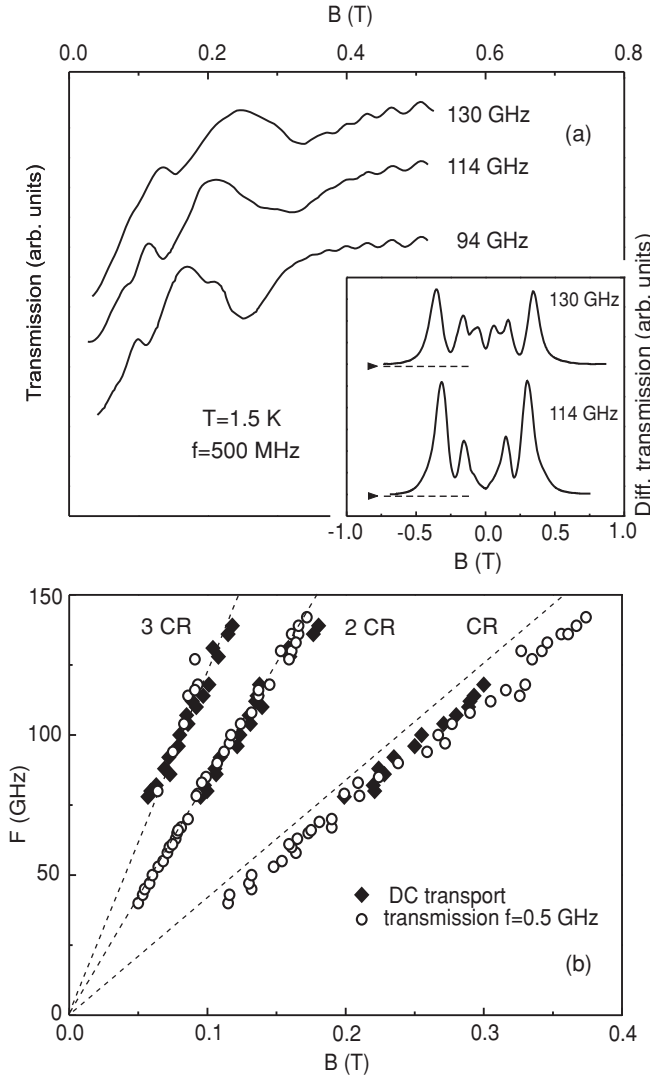


FIG. 2. (a) Dependence of the coplanar waveguide transmission signal on the magnetic field magnitude at a probe signal frequency of  $f = 0.5$  GHz for a series of frequencies of the external microwave irradiation. It should be noted that the curves are shifted for clarity. The inset shows the differential transmission signal for two different microwave irradiation frequencies  $F = 114$  and  $130$  GHz (see text for details). (b) Magnetodispersion of the first three MIRO harmonics. The diamonds correspond to the dc MIRO maxima, and the circles correspond to the transmission signal minima for a probe signal frequency of  $f = 0.5$  GHz. The dashed lines represent the magnetodispersion of the first three harmonics of the cyclotron resonance for an effective electron mass of  $m^* = 0.067m_0$ .

illustrate the similarity of MIRO measured in dc with those observed during high-frequency contactless experiments. The appearance of MIRO in these contactless measurements indicates also the important fact that the presence of ohmic contacts in the 2DES is insignificant for the occurrence of MIRO.

To investigate in detail the MIRO kinetics, we estimate the amplitude of individual coplanar waveguide transmission minima as a function of the probe signal frequency. Owing to their relatively small magnitude, the MIRO-related transmission features can be studied using a double-modulation technique. The high-frequency probe signal is sinusoidally

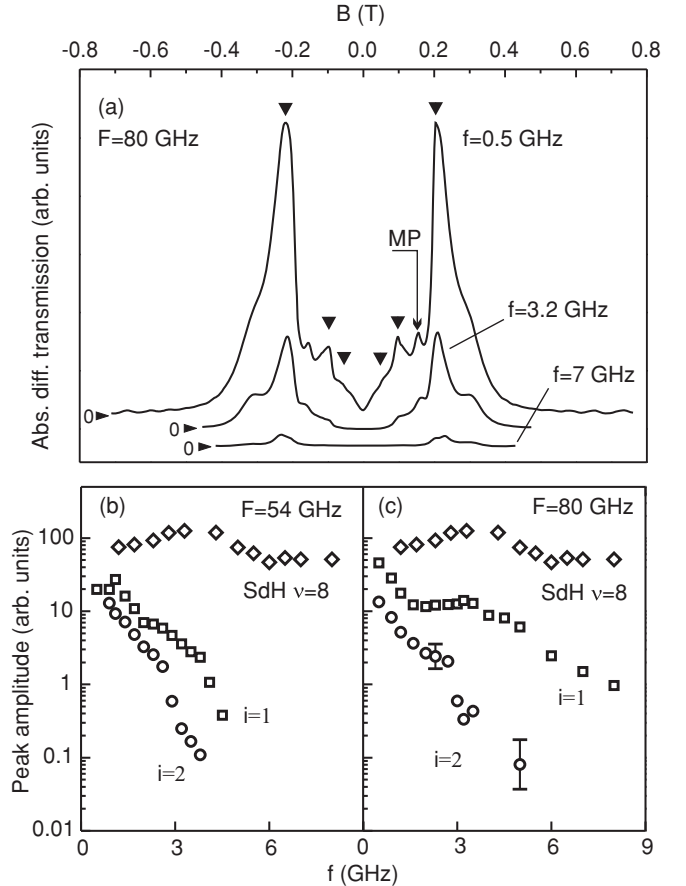


FIG. 3. (a) Absolute value of the differential transmission signal for three different frequencies of the probe signal. The curves are shifted for clarity. The frequency of the external microwave irradiation is set to  $F = 80$  GHz. Vertical arrows indicate the positions of the MIRO maxima. The peak observed in the case of a magnetic field of  $B = 0.16$  T (between the first and the second MIRO harmonics) corresponds to a magnetoplasmon mode (MP). If the magnetic field is higher than  $0.5$  T, Shubnikov-de Haas (SdH) oscillations can be observed. (b) Dependence of the first two MIRO harmonics amplitudes on the probe signal frequency  $f$ . The microwave irradiation frequency is set to  $F = 54$  GHz. For the sake of comparison, the  $f$  dependence of SdH oscillations with a filling factor of  $\nu = 8$  is also shown. (c) Dependence of the first two MIRO harmonics amplitudes on the probe signal frequency  $f$ . The microwave irradiation frequency is set to  $F = 80$  GHz. The  $f$  dependence of SdH oscillations for filling factor  $\nu = 8$  is shown again.

modulated with a frequency of  $2.7$  kHz and detected using a first lock-in amplifier. The output signal, which is proportional to the coplanar waveguide transmission  $T$ , is fed into a second lock-in amplifier. The latter is adjusted to the modulation frequency ( $20$ – $130$  Hz) of the microwave irradiation. This technique has the advantage in that differences in the coplanar transmission with and without microwave irradiation can be directly measured. The inset in Fig. 2(a) shows examples of differential transmission curves for two different microwave irradiation frequencies  $F = 114$  and  $130$  GHz. The differentiation of Eq. (1) shows that the amplitudes of microwave-induced oscillations of the conductivity, magnetoresistance, and differential coplanar waveguide transmission are proportional

to each other. The proportionality holds for the accuracy of factors that depend solely on the magnitude of the magnetic field. Hence, under the assumption given, the above-mentioned amplitudes must be all equally dependent on the frequency of the probe signal.

Figure 3(a) shows the typical magnetic field dependence of the differential coplanar waveguide transmission for various frequencies of the probe signal. The microwave irradiation frequency was fixed at  $F = 80$  GHz. This figure shows well-pronounced MIRO features slightly shifted from the magnetic field values corresponding to different cyclotron resonance harmonics ( $i = 1, 2, 3$ ) as well as a magnetoplasmon mode, located between the first and the second MIRO harmonics. Detailed experiments provide evidence that the magnetoplasmon mode is of bulk nature and characterized by magnetodispersion  $\omega^2(B) = \sqrt{\omega_c^2 + \omega_p^2}$ . Here,  $\omega_p$  is the frequency of the screened plasmon mode<sup>23</sup>

$$\omega_p^2 = \frac{ne^2h}{m^*\varepsilon_0\varepsilon}q^2,$$

where  $\varepsilon_0$  is the vacuum permittivity,  $\varepsilon = 12.8$  is GaAs permittivity, and  $h = 400$  nm is the distance of the 2DES from the top metallized crystal surface. The plasmon wave vector is defined by the width of the Hall bar mesa  $q = N\pi/W$  ( $N = 2, 4, 6, \dots$ ), where  $W$  is a width of the Hall bar used (see schematic in Fig. 1). The even mode numbers come from the geometry of the electric field in the coplanar waveguide. Besides, the observed weak temperature sensitivity confirms plasmon origin of this feature. The amplitude of the plasma resonance decreases by an order of magnitude at temperature  $T = 30$  K, while MIRO features disappear at  $T = 8$  K.

With increasing probe signal frequency  $f$ , the amplitude of the MIRO minima decreases considerably. The decrease is particularly rapid for MIRO harmonics with larger  $i$  factor.

Figures 3(b) and 3(c) show in more detail the dependence of the transmission minima amplitudes on the frequency of the probe signal for microwave irradiation frequencies  $F = 54$  and 80 GHz. They also show the dependence of the amplitude of Shubnikov-de Haas oscillations with a filling factor of  $v = 8$  on the probe signal frequency  $f$  measured by means of the high-frequency coplanar technique. For the sample under discussion, the cyclotron gap for  $v = 8$  is estimated to be equal to 800 GHz and, consequently, an increase in the probe signal frequency up to 10 GHz has a negligible effect on the Shubnikov-de Haas transmission oscillations. On the other hand, transmission features corresponding to the cyclotron resonance harmonics exhibit a strong dependence on the probe signal frequency. For instance, for a microwave irradiation frequency of  $F = 80$  GHz and factor  $i = 1, 2$ , the differential signal decreases by an order of magnitude at probe signal frequencies  $f_1 = 3.0$  GHz and  $f_2 = 1.5$  GHz. The MIRO suppression with increasing probe signal frequency is of significant theoretical interest, but has not yet been explained.

In conclusion, we have applied the contactless high-frequency coplanar technique to study MIRO in a broad frequency range 0.05–10 GHz. We showed that the MIRO features appear in the high-frequency coplanar waveguide transmission as well as in conventional transport measurements. We have also shown that the presence of ohmic contacts in the 2DES is insignificant for the occurrence of MIRO. Finally, according to our experiments, the MIRO amplitude decreases considerably with increasing probe signal frequency and the reduction is faster for MIRO harmonics with larger number  $i$ .

This work was supported by the Russian Foundation for Basic Research (RFBR) and the German BMBF. The authors are grateful to V. A. Volkov and S. I. Dorozhkin for valuable discussions of the experimental results.

\*andreev@issp.ac.ru

<sup>1</sup>M. A. Zudov, R. R. Du, J. A. Simmons, and J. L. Reno, *Phys. Rev. B* **64**, 201311 (2001).

<sup>2</sup>P. D. Ye, L. W. Engel, D. C. Tsui, J. A. Simmons, J. R. Wendt, G. A. Vawter, and J. L. Reno, *Appl. Phys. Lett.* **79**, 2193 (2001).

<sup>3</sup>M. A. Zudov, R. R. Du, L. N. Pfeiffer, and K. W. West, *Phys. Rev. Lett.* **90**, 046807 (2003).

<sup>4</sup>R. G. Mani, J. H. Smet, K. von Klitzing, V. Narayanamurti, W. B. Johnson, and V. Umansky, *Nature (London)* **420**, 646 (2002).

<sup>5</sup>J. H. Smet, B. Gorshunov, C. Jiang, L. Pfeiffer, K. West, V. Umansky, M. Dressel, R. Meisels, F. Kuchar, and K. von Klitzing, *Phys. Rev. Lett.* **95**, 116804 (2005).

<sup>6</sup>S. I. Dorozhkin, I. V. Pechenezhskiy, L. N. Pfeiffer, K. W. West, V. Umansky, K. von Klitzing, and J. H. Smet, *Phys. Rev. Lett.* **102**, 036602 (2009).

<sup>7</sup>C. L. Yang, R. R. Du, L. N. Pfeiffer, and K. W. West, *Phys. Rev. B* **74**, 045315 (2006).

<sup>8</sup>V. I. Ryzhii, *Fizika Tverdogo Tela* **11**, 2577 (1969) [Sov. Phys. Solid State] **11**, 2078 (1970)].

<sup>9</sup>S. I. Dorozhkin, *Pis'ma Zh. Eksp. Teor. Fiz.* **77**, 681 (2003) [JETP Lett. **77**, 577 (2003)].

<sup>10</sup>I. A. Dmitriev, A. D. Mirlin, and D. G. Polyakov, *Phys. Rev. Lett.* **91**, 226802 (2003).

<sup>11</sup>A. D. Chepelianskii and D. L. Shepelyansky, *Phys. Rev. B* **80**, 241308 (2009).

<sup>12</sup>S. A. Mikhailov, e-print [arXiv:1011.1094v2](https://arxiv.org/abs/1011.1094v2).

<sup>13</sup>C. L. Yang, M. A. Zudov, T. A. Knuutila, R. R. Du, L. N. Pfeiffer, and K. W. West, *Phys. Rev. Lett.* **91**, 096803 (2003).

<sup>14</sup>R. L. Willett, L. N. Pfeiffer, and K. W. West, *Phys. Rev. Lett.* **93**, 026804 (2004).

<sup>15</sup>A. A. Bykov, A. K. Bakarov, D. R. Islamov, and A. I. Toropov, *Pis'ma Zh. Eksp. Teor. Fiz.* **84**, 466 (2006) [JETP Lett. **84**, 391 (2006)].

<sup>16</sup>I. V. Andreev, V. M. Muravev, I. V. Kukushkin, J. H. Smet, K. von Klitzing, and V. Umansky, *Pis'ma Zh. Eksp. Teor. Fiz.* **88**, 707 (2008) [JETP Lett. **88**, 616 (2008)].

<sup>17</sup>O. M. Fedorych, M. Potemski, S. A. Studenikin, J. A. Gupta, Z. R. Wasilewski, and I. A. Dmitriev, *Phys. Rev. B* **81**, 201302 (2010).

<sup>18</sup>A. A. Bykov and I. V. Marchishin, *Pis'ma Zh. Eksp. Teor. Fiz.* **92**, 73 (2010) [JETP Lett. **92**, 71 (2010)].

<sup>19</sup>A. A. Bykov, I. V. Marchishin, A. V. Goran, and D. V. Dmitriev, *Appl. Phys. Lett.* **97**, 082107 (2010).

<sup>20</sup>L. W. Engel, D. Shahar, C. Kurdak, and D. C. Tsui, *Phys. Rev. Lett.* **71**, 2638 (1993).

<sup>21</sup>C. P. Wen, *IEEE Trans. Microwave Theory Tech.* **17**, 1087 (1969).

<sup>22</sup>M. A. Zudov, *Phys. Rev. B* **69**, 041304 (2004).

<sup>23</sup>V. M. Muravev, C. Jiang, I. V. Kukushkin, J. H. Smet, V. Umansky, and K. von Klitzing, *Phys. Rev. B* **75**, 193307 (2007).